

Ion ranges and irradiation-induced defects in multiwalled carbon nanotubes

J. A. V. Pomoell, A. V. Krasheninnikov, K. Nordlund, and J. Keinonen
Accelerator Laboratory, University of Helsinki, P.O. Box 43, FIN-00014 Finland

(Received 15 March 2004; accepted 2 June 2004)

Recent experiments on ion irradiation of carbon nanotubes have revealed a wealth of intriguing phenomena. However, in spite of the experimental progress, the production of irradiation-induced defects in multiwalled nanotubes (MWNTs) and their properties are not yet well understood. By employing molecular dynamics with analytical potentials we simulate irradiation of MWNTs with various noble-gas ions and calculate the ion ranges as a function of ion energy. We also use the conventional binary collision stochastic approach to estimate the ranges and compare the results obtained through the two methods. We further characterize the irradiation-induced defects which appear in MWNTs under both single ion impacts and high-dose bombardment. We finally study if, similarly to carbon onions, irradiation can give rise to transformations of nanotubes to nanodiamond rods and demonstrate that such transformations do not occur in MWNTs due to their tubular structure. © 2004 American Institute of Physics. [DOI: 10.1063/1.1776317]

I. INTRODUCTION

Since their discovery in 1991,¹ carbon nanotubes (CNTs) have been envisaged to be the building blocks of a variety of nanoscale devices and materials. For instance, due to their inherent nanometer-size and ability to be either metallic or semiconducting depending on the wrapping angle,² CNTs can be utilized in nanoelectronics. Excellent mechanical characteristics^{2,3} of CNTs suggest their use as structural reinforcements. There are many other promising applications of CNTs.^{2,3} However, to fully exploit all the CNT potentials, effective means of tailoring CNT properties must be developed.

Irradiation of materials with beams of energetic particles (ions and electrons) is a standard and important tool for modifying material properties. Irradiation makes it possible to introduce foreign atoms into the sample, create local amorphous regions or, vice versa, recrystallize the lattice. Depending on the type of the irradiated material and on the characteristics of energetic particles, many other irradiation-mediated modifications are possible.

Irradiation has recently been used to alter the properties of CNTs and thus achieve the wanted functionality. For example, 50 keV Ga⁺ irradiation of multiwalled nanotubes (MWNTs) gave rise to the formation of highly ordered pillboxlike nanocompartments in the tube interior and to changes in the electrical properties of irradiated MWNTs.⁴ Ga⁺ beams have also been used for thinning, slicing, and welding MWNTs at precise locations along the nanotube axis,⁵ and Ar⁺ beams for enhancing the field emission⁶ from MWNTs and making MWNT-based quantum dots⁷ as well as single-electron inverters.⁸

Irradiation-induced changes in the electrical transport properties have been reported for single-walled nanotubes (SWNTs) (Refs. 9–11) as well, which might be important for further progress in carbon-based electronics. Moreover, due to their inherent nanometer-scale and the unique ability to heal the irradiation-induced damage by saturating dangling bonds,¹² SWNTs can be welded together by an electron¹³ or,

in principle, ion¹⁴ beam to form molecular junctions and multiterminal heterostructures. Ion irradiation can also be used for chemical functionalization of nanotubes¹⁵ and for producing amorphous diamond-nanotube composites.¹⁶ Experiments also show that ion bombardment with CNTs as masks against irradiation (to protect the areas under the tubes from sputtering) may be employed for fabricating ultranarrow metal nanowires¹⁷ as an alternative to the conventional electron-beam lithography.

However, even though irradiation is routinely used nowadays for modifying material properties, effects of ion irradiation on CNTs have not yet been fully understood, as the damage creation mechanisms in CNTs substantially differ¹⁸ from those in bulk carbon systems (graphite and diamond), not to mention traditional metals or dielectrics. The knowledge of the microscopic structure of irradiation-induced defects in MWNTs is particularly poor. Although effects of ion irradiation on the electronic characteristics of MWNTs have been studied,^{4,7,8,19–21} the types of defects have not yet been experimentally characterized at the atomic scale. There is also very little information on the ranges of different ions in MWNTs. Finally, at the moment there exists no comprehensive explanation for many irradiation-mediated phenomena, e.g., formation of pillboxlike nanocompartments in the tube interior.⁴

In this paper, we theoretically study irradiation effects in MWNTs. Although production of defects in SWNTs has received considerable attention^{14,22–25} because of the simpler geometry of SWNTs, the damage creation and stopping of energetic ions in MWNTs has not yet been systematically addressed. By employing atomistic computer simulations, we simulate production of defects in MWNTs, and analyze the structure of defects after both single impact of an energetic ion and high-dose irradiation. Because knowing ion ranges in MWNTs has considerable practical importance, we estimate the ability of MWNTs to stop energetic noble-gas ions and consider effects of the highly anisotropic tube atomic structure on the ion ranges and defect distribution.

Finally, since irradiation-induced graphite-to-diamond transformations have been observed in experiments^{26–28} on irradiation of carbon onions—another carbon system with graphitic atomic structure—we address the question whether such transformations can also occur in MWNTs.

II. SIMULATION METHODS

In order to shed light on the behavior of MWNTs under ion irradiation, we utilized classical molecular dynamics (MD) (Ref. 29) with analytical potentials, currently the only method both fast and realistic enough to study production of defects under irradiation in systems consisting of a large amount of atoms while taking explicitly into account the arrangement of atoms in the sample and chemical bonding between them.

Unless specially noted, the interaction between the carbon atoms in the nanotube graphite network was modeled with the Brenner II interatomic potential.³⁰ The Brenner potential was smoothly joined at short interatomic separations with a repulsive potential calculated by density-functional theory methods.³¹ The computationally intensive four-body part of the potential was omitted because it is not of significant importance in these kinds of impact simulations.^{22,25}

The Brenner potential does not take into account van der Waals-type (vdW) interactions between the MWNT shells. Thus, although one can expect that vdW interactions with the typical energies ~ 0.05 eV/atom should play a minor role in collisions of ions and energetic recoils with energies of hundreds of eV, we also employed the Stuart adaptive intermolecular reactive empirical bond order (AIREBO) potential for hydrocarbons.³² The AIREBO model is not just a sum of a short-range covalent potential and a pair-wise van der Waals term. The individual atoms in this model are not constrained to remain attached to specific neighbors, nor to maintain a particular hybridization. Depending on the local atom environment and atom separation, the long-range interaction is switched on/off, which enables the simulation of chemical reactions and defect configurations for which the interplay between covalent and long-range interactions might be important. The interaction between the ions considered (He, Ne, Ar, Kr, and Xe) and the carbon atoms was modeled with the Ziegler-Biersack-Littmark universal repulsive potential.³³

We considered MWNTs composed of armchair nanotubes with chiral indices chosen to provide the intershell separation of 0.32–0.34 nm.² We did not study MWNTs composed of nanotubes with other chiralities, since the behavior of CNTs under irradiation depends on the chirality²⁵ only weakly. We considered only freestanding nanotubes suspended by their ends. Unless specially noted, we randomly chose the ion impact point over the nanotube surface, but the original ion velocity vector was perpendicular to the tube axis. To avoid reflection of pressure waves from the edge of the system, we fixed the boundary atoms and utilized Berendsen temperature quenching³⁴ at the borders of the system during the ion impact. When the collisional phase was over, the velocities of all atoms were slowly scaled to zero. The lengths of our nanotubes were between 5 and 20 nm. The

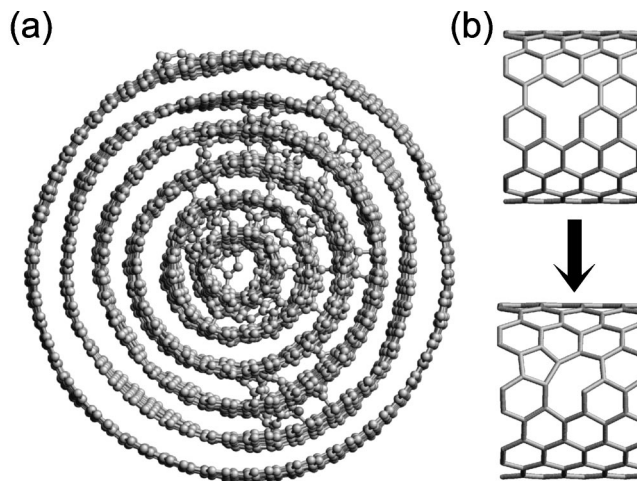


FIG. 1. Typical atomic structure of a MWNT with six shells after a 1.25 keV Xe ion impact. (a) Reconstruction of a single vacancy in a (8,8) armchair single-walled nanotube. (b) Only the front wall is shown.

irradiation simulations were carried out at zero temperature, as we earlier demonstrated that temperature effects are not significant for primary damage production in carbon nanotubes.²⁵ Other details of our simulation methods can be found in Refs. 14, 22–25, and 35.

We also used the standard program SRIM (Ref. 36) to compute ion ranges in MWNTs. Contrary to molecular dynamics, the SRIM code does not explicitly take into account the nature of chemical bonds in the system, but stochastically models the interactions between energetic particles within the binary collision approximation. Also, SRIM treats the irradiated sample as an amorphous structure. Due to these simplifications, the code makes it possible to simulate stopping of energetic ions on micrometer scale, which is beyond the reach of MD because of computational limitations. Thus, the code can be used for higher ion energies (up to the GeV range) which require large simulation cells due to the large typical distance the ions travel in the system before stopping. However, its accuracy remains questionable, especially for highly anisotropic systems and low ion energies. At the same time, SRIM has been used⁴ for evaluating the ion ranges in MWNTs, although its applicability to this problem is not obvious *a priori*. In this paper, we compare our MD simulation results with the corresponding SRIM calculation data to elucidate the applicability of SRIM for simulating ion ranges in CNT samples.

III. RESULTS AND DISCUSSIONS

A. Ion-irradiation-induced defects in MWNTs

The typical atomic network of a six-shell MWNT after the impact of a Xe ion with energy $E_i = 1.25$ keV is shown in Fig. 1(a). The impact resulted in the formation of vacancies on the walls of the MWNT and interstitial atoms between the shells. The vacancies can form new vacancy-related defects by saturating some of the dangling bonds.^{12,22,23,37,38} For a single vacancy, this reconstruction results in the appearance of a pentagon ring accompanied by moving of the dangling bond atom out of the shell by 0.5–0.7 Å, similar to vacancies in graphite,³⁹ see Fig. 1(b). If there are two vacancies in

the adjacent shells (which is frequently the case especially for heavy ions such as Xe), the protruding atoms can give rise to covalent bonds between the shells as in graphite.⁴⁰ Carbon interstitials and interstitial clusters formed due to interstitial diffusion can also bridge the adjacent shells in MWNTs. Irradiation also results in sputtering of carbon atoms, especially in the irradiation direction.

A more detailed analysis of the impacts showed that when an energetic ion collides with the nanotube, it first transfers energy to one-to-three atoms in the uppermost shell, thus creating several primary carbon recoils and a single- or multiple-atom vacancy. The energetic C recoils then produce more recoils as they collide with carbon atoms in other shells, creating more damage together with the ion. As a result, an amorphous region can be formed.

Note that although vacancies can saturate dangling bonds by forming nonhexagonal rings and reducing locally the tube diameter,¹² experiments on irradiation of MWNTs with 3 keV Ar ions followed by x-ray photoelectron spectroscopy and transmission electron microscopy (TEM) probing¹⁹ demonstrated that some carbon dangling bonds were still present, which can be understood in terms of metastability of single- and multiple-atom vacancies.³⁷

TEM investigations of MWNTs irradiated with energetic electrons²⁸ also indicated that point defects and amorphous regions did not anneal at room temperatures, which is quite different from the behavior of point defects in typical semiconductors and metals. In semiconductors like Si a majority of all Frenkel pairs produced are known to recombine below room temperature.⁴¹ In dense metals, nearly all the interstitials and vacancies produced during the ballistic phase of the cascade recombine with each other after only a few picoseconds, regardless of the sample temperature.⁴²

To quantitatively characterize the damage produced by ions in MWNTs with different number of shells, we calculated the coordination defect numbers in single-, double- and triple-walled CNTs after impacts of Ar ions with energies up to $E_i=1.1$ keV. The coordination defect number is simply the number of carbon atoms with coordination other than three. Recall that in a pristine nanotube all carbon atoms are three-fold coordinated (have three nearest neighbors). Thus, the number of atoms with coordinations other than three (atoms near defects) represents a deviation from the pristine atomic structure, i.e., the damage produced in the CNT by the ion.

In Fig. 2 we plot the coordination defect numbers as functions of E_i for CNTs with one, two, and three shells. One hundred impact events were simulated for every energy considered, and the results were averaged. It is evident from Fig. 2 that at low ion energies the damage quickly increases with E_i , as all the ion energy is deposited in the CNT. However, at higher energies the damage increases more slowly, and finally saturates to a certain value which depends on the number of shells in the MWNT. The reason for such behavior is that at high E_i the nuclear collision cross section for defect production drops (see below) and the ion transfers only a part of its energy. To put it in a different way, the ion goes too quickly through the CNT for efficient momentum transfer (unless we have, of course, a head-on collision with one of the carbon atoms, but these events are rare). The damage

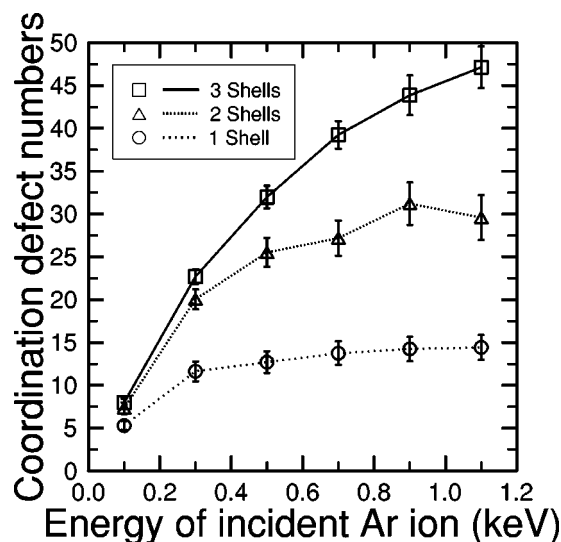


FIG. 2. Coordination defect numbers as functions of the incident Ar ion energy for nanotubes with different numbers of shells.

production in MWNTs is qualitatively the same as in SWNTs,²³ but the number of defects is higher due to a larger number of atoms and thus a higher probability for energy transfer.

B. High-dose ion irradiation

Experiments^{4,19,20} provide evidence that ion irradiation results in gradual amorphization of the nanotube atomic network. Under high-dose irradiation even the MWNTs with originally hollow cores transform to nanorods composed of amorphous carbon. Depending on the ion mass and energy, the irradiated MWNTs become totally amorphous at different doses ranging from 10^{15} cm⁻² for 50 keV Ga⁺ ions up to 4×10^{16} cm⁻² (Ref. 20) and even higher¹⁹ for low-energy Ar ion irradiation.

With respect to high-dose irradiation of MWNTs, one of the most intriguing questions is the possibility of forming diamond nanorods by irradiating the tubes. It is known that high-dose electron^{26,28} and ion²⁷ irradiation of carbon onions whose atomic network also consists of carbon atoms in the sp^2 hybridization, gives rise to the formation of diamond nanocrystals in the onion cores. Because the transformation of graphitelike material to diamond is of considerable technical importance and since diamond nanorods are expected to have unique properties,⁴³ it is interesting if such transformations can occur in MWNTs under irradiation.

To study the behavior of MWNTs under high-dose ion irradiation, we carried out simulations as follows. First an argon ion impact on a MWNT with three shells was modeled as discussed above, then the system temperature was raised to $T=2000$ K and kept for 45 ps, then the system was gradually quenched to 0 K. After that the same procedure was repeated until a desired irradiation dose was obtained. By keeping the system at high temperatures, we partly accounted for annealing of defects at room temperatures, but at macroscopic time scale. The quenching of the system was necessary as we aimed at simulating low-temperature irradiation. One hundred consecutive impacts were modeled, which

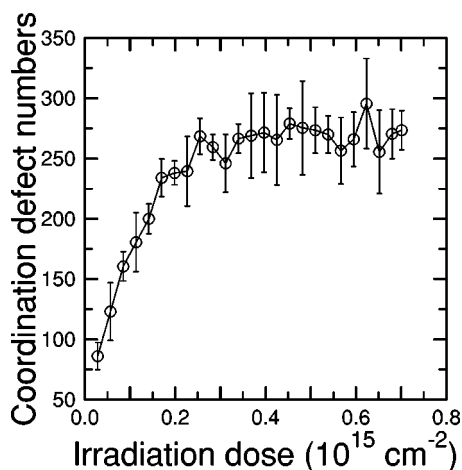


FIG. 3. Coordination defect numbers in a three-shell MWNT as a function of 1 keV Ar ion irradiation dose.

corresponded to a dose of $\Phi = 0.701 \times 10^{15} \text{ cm}^{-2}$. The incident energy of the argon ion was chosen to be $E_i = 1 \text{ keV}$. Due to computational limitations, only six independent runs were carried out, then the results were averaged.

The simulation showed that the damage created in the nanotube quickly increases with the irradiation dose, see Fig. 3. However, at higher irradiation doses the defect numbers saturate toward a constant value. This is because at a certain irradiation dose the system has reached a degree of disorder so large that an incoming energetic ion will not change the internal total coordination numbers substantially. The average bond angle decreased with the dose and saturated toward a value of $\approx 114^\circ$ (see Fig. 4) at higher doses, which is closer to the bond angles in diamond (109°). However, a more detailed coordination and angle analysis showed no evidence for sp^3 hybridization.

We also performed analogous calculations using the Stuart potential. Both simulations gave qualitatively similar results, thus implying that the weak van der Waals interaction between the shells of the MWNT does not play a significant role in these kinds of irradiation processes. Moreover, due to defect-mediated bonds between the shells, the vdW part of

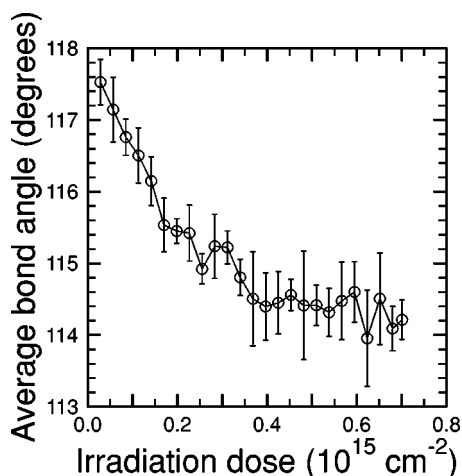


FIG. 4. Average bond angle in a three-shell MWNT as a function of 1 keV Ar ion irradiation dose.

the potential is practically switched off already at a dose of $0.2 \times 10^{15} \text{ cm}^{-2}$. The differences in coordination defect numbers and angles originated mostly from different parametrizations of the covalent short-range part of the potentials.

The absence of the graphite-to-diamond transition can be associated with the tubular shape of MWNTs. For both MWNTs and onions, the pressure in the inner parts of the system increases due to “mending” the vacancies in the graphitic shells and thus decreasing the shell diameter as well as due to growing concentration of carbon atoms in the interior of the tube. However, carbon interstitials, unlike interstitials in spherical onions, can easily migrate away from the regions with the elevated pressure. Thus, the irradiation-mediated increase in pressure proves to be insufficient for the transformation. Experiments^{19,20} on ion irradiation of MWNTs did not provide any evidence for sp^3 hybridization either. Note that Tersoff-like potentials for carbon seem to overestimate the migration barrier for carbon interstitials.⁴⁴ Thus, in reality the escape rate of interstitials from the regions with increased pressure may be even higher than in our simulations. However, even with some “extra” interstitials, we did not observe any evidence for the transformation.

C. MD simulations of stopping of energetic ions in MWNTs

Understanding the ability of MWNTs to slow down energetic atoms and ions is important for several potential applications. Specifically, MWNTs can work as masks¹⁷ against irradiation, or the other way around, for spatially selective ion implantation into areas of the substrate not covered by the tube. An important issue is thus to know the penetration depth of an ion with a certain energy into the MWNT.

In order to estimate the ability of MWNTs to stop energetic ions of different masses, we performed MD simulations as described earlier, by modeling irradiation of nanotubes consisting of one to six shells. Various noble gas ions were considered. For every impact event we calculated the number of recoils (both carbon and ion) with energy $E > 50 \text{ eV}$ which appeared under the nanotube. Recoils with lower energies should create very little damage in the substrate under the tube and can essentially be discarded. We performed 100–300 simulation runs for each ion energy and CNT considered and averaged the results.

The average number of energetic recoils per incoming Xe ion as a function of the incident ion energy is presented in Fig. 5. As can be seen, the recoils appear at a certain threshold energy E_{th} which depends on the number of shells, then the number of recoils increases with the incident Xe ion energy. The same behavior has been previously reported for Ar ions.³⁵ We stress that E_{th} (the minimum energy for recoils to appear *under* the tube) is a quantity different from the displacement energy (the minimum kinetic energy which should be transferred to a carbon atom to leave its original position in the nanotube atomic network without immediate recombination).

We ran similar simulations for other noble-gas ions. From our data, we estimated the threshold energy needed to produce energetic recoils under the nanotube. E_{th} as a function of the number of shells, or correspondingly, the outer

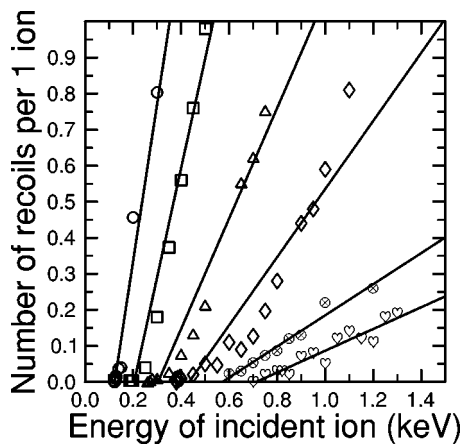


FIG. 5. Numbers of recoils as functions of the energy of incident Xe ions for nanotubes with various numbers of shells. Symbols \circ correspond to nanotubes with one shell, \square to double-walled (two-shell) nanotubes, Δ (3), \diamond (4), \otimes (5), and \heartsuit (6). Solid lines are linear fits to the MD data.

diameter, is given in Fig. 6. To ease comprehension, we did not show in Fig. 6 the error bars resulting from the statistical errors in linear approximation of the MD data presented in Fig. 5.

It is seen from Fig. 6 that in the energy range considered, the threshold energy grows linearly with the number of shells for each ion. It is also evident that the threshold energy does not increase monotonically with the mass of the ion. E_{th} for Xe, the heaviest ion, lies between the respective values for Ne and Ar. But in general, apart from Xe, E_{th} increases with the mass of the ion, as expected. The threshold energies for He are much lower than for any other ions considered.

In order to understand such a behavior, in Fig. 7 we plot the cross section for the defect production as a function of the energy of incident ions.⁴⁵ We evaluated the cross sections $S = \pi p^2$ for different ions by calculating the maximum impact parameter p for which an ion transfers at least 25 eV (the minimum kinetic energy for displacing an atom in the nanotube in our MD model) to a C atom in a binary collision (see Eqs. 2-62, and 2-64 in Ref. 33).

As shown in Fig. 7, the cross section for He is very small, which explains why the threshold energy is so low in

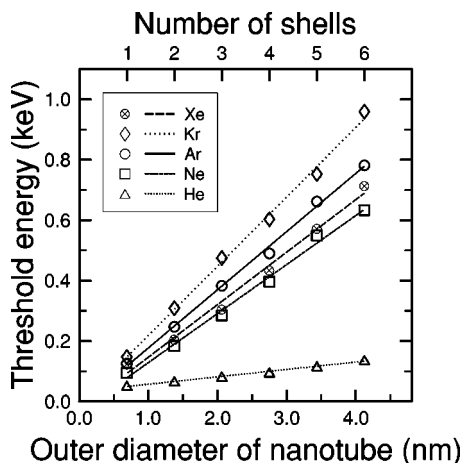


FIG. 6. Threshold energy of noble-gas ions as a function of the multiwalled nanotube outer diameter and, correspondingly, the number of shells.

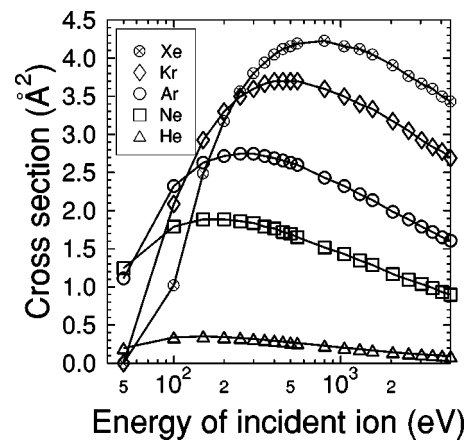


FIG. 7. Cross section for the defect production in nanotubes as a function of incident ion energy for various ions.

the case of He irradiation. Basically, it means that He ions easily go through the tube and hit the substrate directly. However, it should be pointed out that our MD simulations take into account the nuclear stopping only, while for He the electronic stopping should be essential even for energies below 1 keV. Thus, one can expect somewhat higher values for E_{th} .

It is also evident from Fig. 7 that for low (<0.2 keV) energies the cross section for Xe is smaller than those for Ar and Kr, which gives rise to lower values of E_{th} . In general, the cross sections averaged over the energy range of 0–1 keV are roughly the same for all ions (except for He). Thus, the difference in E_{th} for ions with the same energy but different masses is relatively small—about 30%, although Xe is much heavier than, e.g., Ne. However, since at high (>5 keV) energies the cross section is directly proportional to the ion mass (see Fig. 7), one can expect that the threshold energy should also scale linearly with the ion mass. Due to computational limitations on the simulation time and the size of the system (which should be much larger at high ion energies as the ion penetrates deeper into the system), we were unable to access high ion energies with MD. Instead, we used the binary collision approach implemented in the simulation code SRIM, see below.

The data presented in Fig. 6 can also be used for evaluating the ion ranges in MWNTs. The maximum penetration depth of energetic recoils is, in general, different from the ion range. Although, as mentioned above, a 50 eV recoil creates very little damage which at room temperature can easily anneal, the ion can penetrate slightly deeper into the sample. Thus, the data presented in Fig. 6 are the lower bound on the ion range. This implies that, e.g., a Kr ion with an energy of 1 keV will penetrate through ≈ 12 graphitic layers (six shells) or a bit more before complete stopping, which corresponds to ~ 4 nm. Detailed analysis of the maximum penetration depth of C energetic recoils and ions for different impact energies and various ions showed that maximum penetration depths of energetic recoils and ion ranges are indeed close to each other.

Finally, to understand the effects of the nanotube tubular structure on the ion ranges, we considered off-normal (with respect to the tube axis) incidence of ions. We simulated

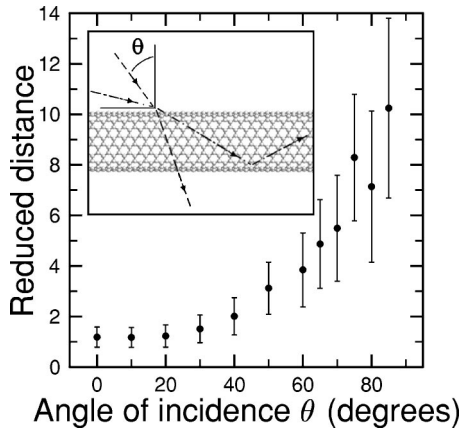


FIG. 8. Average reduced distance (ratio distance/tube diameter) the 1 keV Ar ion travels along the axis of a (10,10) SWNT as a function of the ion incidence angle. The inset shows possible trajectories for the impinging ion at two different angles of incidence.

impacts of 1 keV Ar ions on a (10,10) SWNT. The impact points were randomly chosen. Various angles of incidence were considered, see the inset in Fig. 8. We evaluated the average distance the ion travels *inside* the tube during a finite-time simulation. In Fig. 8 we present the reduced distance (a ratio of the traveled distance to the tube diameter) as a function of angle θ . It is evident that for $\theta < 50^\circ$ the ion easily penetrates right through the tube, while for $\theta > 50^\circ$ the ion remains inside the tube and travels along the tube axis tens or even hundreds of nanometers with a very small loss of energy (~ 1 eV) per every collision with the SWNT wall. Note that at the normal incidence the 1 keV ion goes no more than 5 nm deep into the MWNT, see Fig. 6. Thus, the actual penetration depth into the nanotube sample can be much more than the corresponding value for the case of ion normal incidence.

D. Ranges of energetic ions in MWNTs calculated within the framework of the binary collision approximation

As mentioned above, the standard program SRIM (Ref. 36) which treats the irradiated sample as an amorphous structure can be used for estimating the ion ranges at ion energies inaccessible in MD simulations. Thus, we also employed the SRIM code to calculate the maximum penetration depth of ions with different masses into a carbon sample. We let the sample have the same density as the typical MWNT in our MD simulations, and let the displacement threshold for a carbon in the network be $E_d = 25$ eV (the threshold energy for displacing an atom in the nanotube in our MD model), otherwise we used the default input parameters. We also varied all input parameters to see if the results were sensitive to the choice of values. No significant sensitivity was observed.

We ran two different sets of SRIM simulations. In the first set, for the direct juxtaposition with the MD simulations described above we varied the sample thickness and determined the one needed to slow down an energetic ion to 50 eV. This thickness can be interpreted as the maximum penetration depth of energetic ions/recoils, or the maximum damage range. The maximum penetration depths of ions still

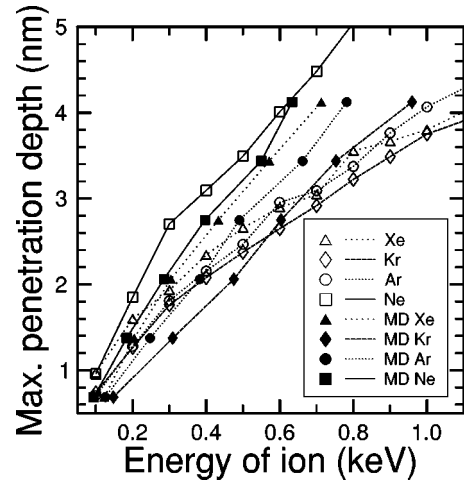


FIG. 9. Maximum penetration depth of energetic ions as a function of incident ion energy calculated with the SRIM code. Lines are guides for the eye. For comparison the corresponding MD data are also shown.

having an energy of 50 eV as a function of ion energy are presented in Fig. 9. It is evident that the SRIM results are in line with the MD data. The difference between the corresponding MD and SRIM data is about 30%. As in the MD simulations, for low ion energies the penetration depth of Xe ions is higher than for Ne and Ar, which can also be understood in terms of the behavior of the cross section for the nuclear stopping.

In the second set of our SRIM simulations we calculated the ion ranges by defining the range, as usual, as the maximum penetration depth of the ion into a macroscopically thick sample for different noble-gas ions with energies up to 20 keV. The results are given in Fig. 10. At high ion energies ($E_i > 1$ keV) both types of simulations gave essentially the same results. For $E_i < 1$ keV the second set of imulations gave slightly higher ranges, as expected.

The reasonably good agreement between the MD and binary collision results indicates that the SRIM code can be employed for estimating the ranges of ions *inside* MWNTs provided that the initial velocity vector of the ion is perpendicular to the tube axis. One can expect that for higher ion

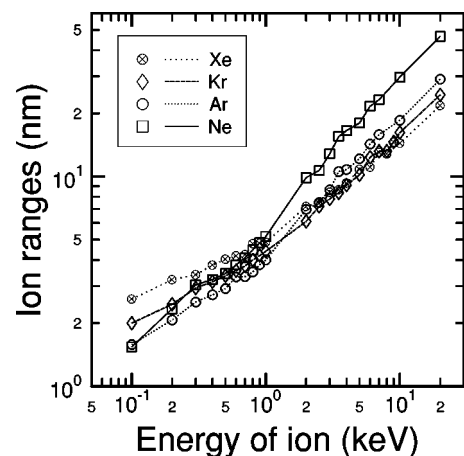


FIG. 10. Noble-gas ion ranges as a function of incident ion energy calculated with the SRIM code. Lines are guides for the eye. Note the logarithmic scale used.

energies the SRIM code should work even better, as the atomic structure of the sample becomes less important.

However, for off-normal ion incidence the ranges could be several orders of magnitude larger due to high anisotropy of CNTs and open channels inside the MWNTs, especially in their inner hollow parts. Thus, the stochastic approach and binary collision approximation can hardly be used in this case. This is not surprising, since the SRIM code neglects the atomic structure and thus it cannot take into account the channeling effects, although these effects can be very important in ion propagation through CNTs, especially for high ion energies.^{46,47}

Note that *macroscopic* CNT samples usually are agglomerations of randomly aligned CNTs as, e.g., in the raw product or purified nanotube bucky paper.^{48,49} Thus, the actual ranges of ions, i.e., how deep the ions penetrate into the sample can differ from the ion ranges inside the tubes due to ion channeling. Moreover, since the averaged sample density can be two to three orders of magnitude lower than the density of nanotubes due to the voids between tangled or even aligned CNTs, it is difficult to estimate the ion ranges with respect to the sample surface. Instead, it is more expedient to speak about ranges of ions inside MWNTs or SWNT bundles.

IV. CONCLUSIONS

Making use of the MD method with analytical potentials, we simulated impacts of energetic noble-gas ions onto MWNTs. We demonstrated that irradiation gives rise to the formation of vacancies on shells of MWNTs and intershell links which appear as a result of the saturation of dangling bonds at carbon interstitials and atoms nearby the vacancies. The formation of such links under irradiation of closely related systems—bundles of single-walled nanotubes—has recently been demonstrated experimentally.⁵⁰ As the links resulted in the reinforcement of the irradiated bundles, one can expect that irradiation of MWNTs should also increase the overall MWNT mechanical properties by transferring the mechanical load to the inner shells which do not contribute to the axial reinforcement in pristine MWNTs due to very weak intershell interactions.^{51–53}

We further modeled high-dose ion irradiation of MWNTs. We found that irradiation gives rise to a quick amorphization of MWNTs. Unlike closely related structures with graphitic arrangement of atoms—carbon onions—MWNTs do not form nanodiamonds under irradiation. The absence of the graphite-to-diamond transition can be associated with the tubular shape of MWNTs, which makes it possible for the interstitials to easily escape from the regions with irradiation-increased pressure.

Finally, using MD and the conventional binary collision stochastic approach implemented in the code SRIM, we calculated noble-gas ion ranges in MWNTs. We showed that if the initial ion velocity vector is oriented perpendicular to the tube axis as, e.g., in experiments on ion irradiation of individual MWNTs (Ref. 7 and 8), the MD and SRIM results are in a good agreement. Thus, although MWNTs are highly anisotropic materials, the SRIM code can be used for estimat-

ing the ion ranges at normal incidence of the ions. This result is particularly important as SRIM has been repeatedly used for estimating the irradiation-induced damage in MWNTs, although the code applicability is not clear *a priori* due to nanometer size and highly anisotropic structure of MWNTs.

However, if the angle between the ion velocity vector and tube axis is small, the SRIM code fails, as incident ions with even relatively low energies can travel hundreds of nanometers through the empty cores of MWNTs. Efficient ion channeling through the inner cores of MWNTs can be used for creating principally new devices for ion beam steering at the nanoscale. The studies on heavy ion channeling in MWNTs are underway.

ACKNOWLEDGMENTS

Authors would like to thank Professor F. Banhart and Professor S. Stuart for fruitful discussions and cooperation. The research was supported by the Academy of Finland under Project Nos. 48751, 50578, and 202737. Grants of computer time from the Center for Scientific Computing in Espoo, Finland are gratefully acknowledged.

¹S. Iijima, *Nature* (London) **354**, 56 (1991).

²*Carbon Nanotubes, Synthesis, Structure, Properties, and Applications*, edited by M. S. Dresselhaus, G. Dresselhaus, and P. Avouris (Springer, Berlin, 2001).

³R. H. Baughman, A. A. Zakhidov, and W. A. de Heer, *Science* **297**, 787 (2002).

⁴B. Q. Wei, J. D'Arcy-Gall, P. M. Ajayan, and G. Ramanath, *Appl. Phys. Lett.* **83**, 3581 (2003).

⁵M. S. Raghuvver, P. G. Ganesan, J. D'Arcy-Gall, G. Ramanath, M. Marshall, and I. Petrov, *Appl. Phys. Lett.* **84**, 4484 (2004).

⁶D.-H. Kim, H.-S. Jang, C.-D. Kim, D.-S. Cho, H.-D. Kang, and H.-R. Lee, *Chem. Phys. Lett.* **378**, 232 (2003).

⁷M. Suzuki, K. Ishibashi, K. Toratani, D. Tsuya, and Y. Aoyagi, *Appl. Phys. Lett.* **81**, 2273 (2002).

⁸K. Ishibashi, D. Tsuya, M. Suzuki, and Y. Aoyagi, *Appl. Phys. Lett.* **82**, 3307 (2003).

⁹J. W. Park, J. Kim, J.-O. Lee, K. C. Kang, J.-J. Kim, and K.-H. Yoo, *Appl. Phys. Lett.* **80**, 133 (2002).

¹⁰H. Stahl, J. Appenzeller, R. Martel, P. Avouris, and B. Lengeler, *Phys. Rev. Lett.* **85**, 5186 (2000).

¹¹C. Mikó, M. Milas, J. W. Seo, E. Couteau, N. Barisić, R. Gaál, and L. Forró, *Appl. Phys. Lett.* **83**, 4622 (2003).

¹²P. M. Ajayan, V. Ravikumar, and J.-C. Charlier, *Phys. Rev. Lett.* **81**, 1437 (1998).

¹³M. Terrones, F. Banhart, N. Grobert, J.-C. Charlier, H. Terrones, and P. Ajayan, *Phys. Rev. Lett.* **89**, 075505 (2002).

¹⁴A. V. Krasheninnikov, K. Nordlund, J. Keinonen, and F. Banhart, *Phys. Rev. B* **66**, 245403 (2002).

¹⁵B. Ni, R. Andrews, D. Jacques, D. Qian, M. B. J. Wijesundara, Y. Choi, L. Hanley, and S. B. Sinnott, *Appl. Phys. A: Mater. Sci. Process.* **105**, 12719 (2001).

¹⁶H. Schittlenhelm, D. B. Geohegan, G. E. Jellison, A. A. Puzos, M. J. Lance, and P. F. Britt, *Appl. Phys. Lett.* **81**, 2097 (2002).

¹⁷W. S. Yun *et al.*, *J. Vac. Sci. Technol. A* **18**, 1329 (2000).

¹⁸A. V. Krasheninnikov and K. Nordlund, *Nucl. Instrum. Methods Phys. Res. B* **216**, 355 (2004).

¹⁹Y. Zhu, T. Yi, B. Zheng, and L. Cao, *Appl. Surf. Sci.* **137**, 83 (1999).

²⁰P. Vincent, A. Brioude, C. Journet, S. Rabaste, S. T. Purcell, J. L. Brusqu, and J. C. Plenet, *J. Non-Cryst. Solids* **311**, 130 (2002).

²¹A. K. Chakraborty, R. A. J. Woolley, V. R. Dhanak, and M. R. C. Hunt, (unpublished).

²²A. V. Krasheninnikov, K. Nordlund, M. Sirviö, E. Salonen, and J. Keinonen, *Phys. Rev. B* **63**, 245405 (2001).

²³A. V. Krasheninnikov, K. Nordlund, and J. Keinonen, *Phys. Rev. B* **65**, 165423 (2002).

²⁴E. Salonen, A. V. Krasheninnikov, and K. Nordlund, *Nucl. Instrum. Meth-*

- ods Phys. Res. B **193**, 603 (2002).
- ²⁵J. Pomoell, A. V. Krasheninnikov, K. Nordlund, and J. Keinonen, Nucl. Instrum. Methods Phys. Res. B **206**, 18 (2003).
- ²⁶F. Banhart and P. M. Ajayan, Nature (London) **382**, 433 (1996).
- ²⁷P. Wesolowski, Y. Lyutovich, F. Banhart, H. D. Carstanjen, and H. Kronmüller, Appl. Phys. Lett. **71**, 1948 (1997).
- ²⁸F. Banhart, Rep. Prog. Phys. **62**, 1181 (1999).
- ²⁹M. P. Allen and D. J. Tildesley, *Computer Simulation of Liquids* (Oxford University Press, Oxford University, London, 1989).
- ³⁰D. W. Brenner, Phys. Rev. B **42**, 9458 (1990).
- ³¹K. Nordlund, N. Runeberg, and D. Sundholm, Nucl. Instrum. Methods Phys. Res. B **132**, 45 (1997).
- ³²S. J. Stuart, A. B. Tutein, and J. A. Harrison, J. Chem. Phys. **112**, 6472 (2000).
- ³³J. F. Ziegler, J. P. Biersack, and U. Littmark, *The Stopping and Range of Ions in Matter* (Pergamon, New York, 1985).
- ³⁴H. J. C. Berendsen, J. P. M. Postma, W. F. van Gunsteren, A. DiNola, and J. R. Haak, J. Chem. Phys. **81**, 3684 (1984).
- ³⁵A. V. Krasheninnikov, K. Nordlund, and J. Keinonen, Appl. Phys. Lett. **81**, 1101 (2002).
- ³⁶Program TRIM (2003) by J. F. Ziegler and J. P. Biersack, <http://www.srim.org>
- ³⁷A. V. Krasheninnikov and K. Nordlund, J. Vac. Sci. Technol. B **20**, 728 (2002).
- ³⁸A. J. Lu and B. C. Pan, Phys. Rev. Lett. **92**, 105504 (2004).
- ³⁹A. A. El-Barbary, R. H. Telling, C. P. Ewels, M. I. Heggie, and P. R. Briddon, Phys. Rev. B **68**, 144107 (2003).
- ⁴⁰R. Telling, C. Ewels, A. El-Barbary, and M. Heggie, Nat. Mater. **2**, 333 (2003).
- ⁴¹P. Partyka, Y. Zhong, K. Nordlund, R. S. Averback, I. K. Robinson, and P. Ehrhart, Phys. Rev. B **64**, 235207 (2002).
- ⁴²T. Diaz de la Rubia, R. S. Averback, R. Benedek, and W. E. King, Phys. Rev. Lett. **59**, 1930 (1987); see also Phys. Rev. Lett. **60**, 76(E) (1988).
- ⁴³O. Shenderova, D. Brenner, and R. S. Ruoff, Nano Lett. **3**, 805 (2003).
- ⁴⁴A. V. Krasheninnikov, K. Nordlund, P. O. Lehtinen, A. S. Foster, A. Ayuela, and R. M. Nieminen, Phys. Rev. B **69**, 73402 (2004).
- ⁴⁵These data have been published in an earlier paper (Ref. 25) on the irradiation effects in SWNTs. However, because the cross-section data are essential for understanding the MD results for MWNTs, we also present here the data for the ions considered.
- ⁴⁶S. Bellucci, V. M. Biryukov, Y. A. Chesnokov, V. Guidic, and W. Scandale, Nucl. Instrum. Methods Phys. Res. B **202**, 236 (2003).
- ⁴⁷Y.-N. Wang and Z. L. Mišković, Phys. Rev. A **66**, 042904 (2002).
- ⁴⁸R. H. Baughman *et al.*, Science **284**, 1340 (1999).
- ⁴⁹A. Rinzler *et al.*, Appl. Phys. A (Materials Science & Processing) **67**, 29 (1998).
- ⁵⁰A. Kis *et al.*, Nat. Mater. **3**, 63 (2004).
- ⁵¹J. Cummings and A. Zettl, Science **289**, 602 (2000).
- ⁵²M. Yu, B. I. Yakobson, and R. S. Ruoff, J. Phys. Chem. B **104**, 8764 (2000).
- ⁵³A. N. Kolmogorov and V. H. Crespi, Phys. Rev. Lett. **85**, 4727 (2000).